A model test on an open-cut tunnel structure under the effect of a stick-slip normal fault

Zhiqiang Zhang, Xingyu Zhu and Ronghua Wei
School of Civil Engineering, Southwest Jiaotong University, Chengdu, China and Key Laboratory of Transportation Tunnel Engineering, Ministry of Education, Southwest Jiaotong University, Chengdu, China

Received 10 August 2022
Revised 19 September 2022
Accepted 11 October 2022

Abstract

Purpose – Large displacement misalignment under the action of active faults can cause complex three-dimensional deformation in subway tunnels, resulting in severe damage, distortion and misalignment. There is no developed system of fortification and related codes to follow. There are scientific problems and technical challenges in this field that have never been encountered in past research and practices.

Design/methodology/approach – This paper adopted a self-designed large-scale active fault dislocation simulation loading system to conduct a similar model test of the tunnel under active fault dislocation based on the open-cut tunnel project of the Urumqi Rail Transit Line 2, which passes through the Jiujiawan normal fault. The test simulated the subway tunnel passing through the normal fault, which is inclined at 60°. This research compared and analyzed the differences in mechanical behavior between two types of lining section: the open-cut double-line box tunnel and the modified double-line box arch tunnel. The structural response and failure characteristics of the open-cut segmented lining of the tunnel under the stick-slip part of the normal fault were studied.

Findings – The results indicated that the double-line box arch tunnel improved the shear and longitudinal bending performance. Longitudinal cracks were mainly distributed in the baseplate, wall foot and arch foot, and the crack position was basically consistent with the longitudinal distribution of surrounding rock pressure. This indicated that the longitudinal cracks were due to the large local load of the cross-section of the structure, leading to an excessive local bending moment of the structure, which resulted in large eccentric failure of the lining and formation of longitudinal cracks. Compared with the ordinary box section tunnel, the improved double-line box arch tunnel significantly reduced the destroyed and damage areas of the hanging wall and footwall. The damage area and crack length were reduced by 39 and 59.3%, respectively. This indicates that the improved double-line box arch tunnel had good anti-sliding performance.

Originality/value – This paper adopted a self-designed large-scale active fault dislocation simulation loading system to conduct a similar model test of the tunnel under active fault dislocation. This system increased the similarity ratio of the test model, improved the dislocation loading rate and optimized the simulation scheme of the segmented flexible lining and other key factors affecting the test. It is of great scientific significance and engineering value to investigate the structure of subway tunnels under active fault misalignment, to study its

Funding: The study was funded by the High Speed Railway and Natural Science United Foundation of China [Award number: U1934213] and the General Program of National Natural Science Foundation of China [Award number: 51878572].

Data availability: The data used to support the findings of this study are available from the corresponding author upon request.

Conflict of interest: The authors declare that there is no conflict of interest regarding the publication of this paper.

Railway Sciences
Vol. 1 No. 2, 2022
pp. 169-192
Emerald Publishing Limited
e-ISSN: 2755-0915
p-ISSN: 2755-0907
DOI 10.1108/RS-08-2022-0023

force characteristics and damage modes, and to provide a technical reserve for the design and construction of subway tunnels through active faults.

Keywords Normal fault, Stick-slip, Open-cut tunnel, Model test, Failure characteristics
Paper type Research paper

1. Introduction

With the rapid development of China's economy and society, the development and utilization of urban underground space is expanding, and the construction of subway extensions is accelerating. The layout of the urban subway in China is expanding from coastal to inland areas, but the geological conditions in the western region are very complex, causing problems in the construction of urban subways (Jeon *et al.*, 2004). Subway tunneling through complex geological structures, such as active faults, has become a regular significant project; and scientific design, safe construction and disaster prevention and mitigation of related tunneling projects have become the increasing focus for tunnel contractors (Zheng, Jiang, & Li, 2013). The permanent deformation caused by relative offset between the two sides (hanging wall and footwall) of the fault plane adversely affects underground lifeline works, especially linear structures such as urban metro systems, tunnels in mountains and underground pipelines, and even results in collapse, dislocation or other destructive disasters (Wang *et al.*, 2019; Zhang *et al.*, 2018).

Cases of tunnel damage due to active fault misalignment have increased in recent years. Large displacement misalignment under the action of active faults can cause complex three-dimensional deformation in subway tunnels, resulting in severe damage, distortion and misalignment. There is no developed system of fortification and related codes to follow. There are scientific problems and technical challenges in this field that have never been encountered before (Jiang, Li, & Lin, 2008). Due to long extension of tunnel lines, complex and variable forms of fault distribution, and social and economic goals regarding tunnel works, it is unrealistic to modify tunnel lines to avoid fault zones completely (Kim *et al.*, 2020; Zhao & Yang, 2019). Therefore, it is of great scientific significance and practical engineering value to investigate the structure of subway tunnels under active fault misalignment, study its force characteristics and damage modes and provide a technical reserve for the design and construction of subway tunnels through active faults.

Active faults can be divided into stick-slip faults and creep faults according to the characteristics of fault movement (Allen *et al.*, 1991; Mcgarr & Fletcher, 2003; Sibson, 1977). Between them, the hanging wall and the footwall of the stick-slip fault remain static and accumulate potential energy over a long time. When a weak surface of the fracture zone reaches the rock's ultimate strength, a large dislocation occurs instantaneously; and the dislocation speed is fast and destructive (Abers, 2009; Byerlee & Brace, 1968; Lecomte, Le Pourhiet, & Lacombe, 2012; Ohnaka, 1973). Creep fault is a form of continuous stratigraphic dislocation; its rate is very slow, generally measured in millimeters per year, without burst damage. The stick-slip fault can lead to severe permanent deformation of the strata over a short period of time and is accompanied by ground motion. In tunnel engineering, ground motion is not the main reason for instability and failure near the fault dislocation surface. Massive relative displacement and dislocation of the strata on both sides of the fault surface (the hanging wall and the footwall) are the prime factors for serious damage and the overall collapse of the tunnel (Anastasopoulos *et al.*, 2008; Cui, 2014).

Many scholars have conducted extensive research on the propagation law of stratum fracture surface under the action of a stick-slip fault. Many researchers studied the deformation of strata and fracture propagation caused by reverse fault dislocation through centrifugal tests (Bray, Seed, Ciuff, Members, & Bolton Seed, 1994; Lin, Chung, & Jeng, 2006;

Roth, Scott, & Austin, 1981; Taniyama & Watanabe, 2002). Through numerical analyses and centrifugal tests, Anastasopoulos, Gazetas, Bransby, Davies, and El Nahas (2007) studied the propagation law of the stratum fracture surface caused by normal fault dislocation. The study indicated that the dip angle of the fracture surface caused by normal fault dislocation would gradually increase as it extended to the surface. Lee and Hamada (2005) studied the prediction method of fracture propagation trajectory under normal fault dislocation through a centrifugal test. The results showed that the measurement accuracy of the surrounding rock pressure has greatly influenced the test results, and the test results of a small-scale model had certain defects.

Scholars have also researched the mechanical response characteristics of a cross-fault tunnel structure under stick-slip fault dislocation. Burridge, Scott, and Hall (1989) studied the internal structural forces, such as deformation, bending moment and shear force under fault dislocation through a centrifugal test, and compared the forces with the numerical analysis results. Liu, Li, Sang, and Lin (2015) studied the mechanical response characteristics of tunnel structures under different dip angles of normal faults through similar indoor model tests. Using numerical analysis, Anastasopoulos *et al.* (2008) studied the stress characteristics of a tunnel structure in ground motion after normal fault dislocation. Karamitros, Bouckovalas, and Kouretzis (2007) predicted the structural stress–strain distribution characteristics of buried steel pipes affected by normal fault dislocation through theoretical derivation and analysis. Süleyman (2002) proposed an articulated design of a tunnel based on design and construction aspects. From the perspective of geometric deformation and load distribution, the articulated tunnel structure is believed to reduce the internal force and adapt to larger fault dislocation, but there is no quantitative research such as an experimental demonstration. Shahidi and Vafaeian (2005) used numerical analysis to study the longitudinal deformation characteristics of tunnel structure under the action of normal fault dislocation. Johansson and Konagai (2007) studied the damage to the tunnel from permanent stratum deformation caused by faults and proposed that the influence of the horizontal pressure and moisture content of the stratum should be considered when calculating the energy of stratum dislocation.

However, existing research in China and abroad is still insufficient in terms of testing; the test dislocation rate does not match the actual rate caused by the unclear boundary between stick-slip and creep dislocations. In addition, there are few studies on large-scale model tests. Small-scale model tests are often used to study fault dislocation, but it can be difficult to consider the influence of fault boundary conditions and gravity effects.

In view of these problems, this paper adopted a self-designed large-scale active fault dislocation simulation loading system to conduct a similar model test of the tunnel under active fault dislocation. This system increased the similarity ratio of the test model, improved the dislocation loading rate and optimized the simulation scheme of the segmented flexible lining and other key factors affecting the test. The device was used to study the failure mode of the subway tunnel crossing the Jiujiawan open-cut normal fault (dip angle 60°), and this paper has compared and analyzed the mechanical behavior differences between the two tunnel lining section types: the open-cut double-line box and the modified double-line box arch. The deformation and stress characteristics, failure process, failure characteristics and failure range were comprehensively studied.

2. Engineering background

Urumqi Rail Transit Line 2 is the main skeleton line in the south-northwest direction of the Urumqi Rail Transit network. Line 2 begins at Yan'an Road Station in the south and ends at Huashan Street Station in the north. The total length of the planned line is 19.1 km, with 16

stations in total. In the main urban area of Urumqi, Line 2 passes four active faults: Bagang-Shihua buried fault, Jiujiawan fault group, Xishan fault, and Yamalik fault, as shown in Figure 1.

The Jiujiawan fault group is mainly distributed on the plateau to the northeast side of Xishan. The fault group is the secondary fault within the fault block of the Xishan uplift. The main fault is the slip surface in the Jurassic coal measures with a depth of about 10 km under the fold stratum, which is a Holocene active fault. It is mainly composed of four normal faults that strike 60°N–65°E and are laid out in an equidistant parallel arrangement. The four faults are F_{j1}, F_{j2}, F_{j3} and F_{j4}, from north to south, respectively. The length of a single fault zone is 3–5 km. The section in the south of each normal fault zone tends to be northwest, with an inclination angle of over 70°. The normal fault section in the north tends to be southeast, with an inclination angle of over 50°, forming an asymmetric graben structure. The south branch fault is the main fault, and the north branch fault is the secondary fault.

The interval between Huashanjie Station and Urumqi Station of the Urumqi Subway Line 2 passes through the third fault F_{j3} of the Jiujiawan fault group. Its dislocation mode is shown in Figure 2. The fault can be clearly observed near the foundation pit under construction, as shown in Figure 3. Considering the possibility of unexpected events in the next 100 years, it has been suggested that the vertical dislocation of the fault should be 75 mm. Because of the shallow-buried depth of the tunnel at the fault (10–18 m), the open-cut method was used in construction, and the cross-sectional shape of the tunnel is double-line box section type, which can improve the shear and longitudinal bending performance.

3. Experimental design

3.1 Experimental system

At present, research with fault rupture model experiments mainly adopts small-scale tests, but these small-scale model tests have the following deficiencies. Because of its small scale,

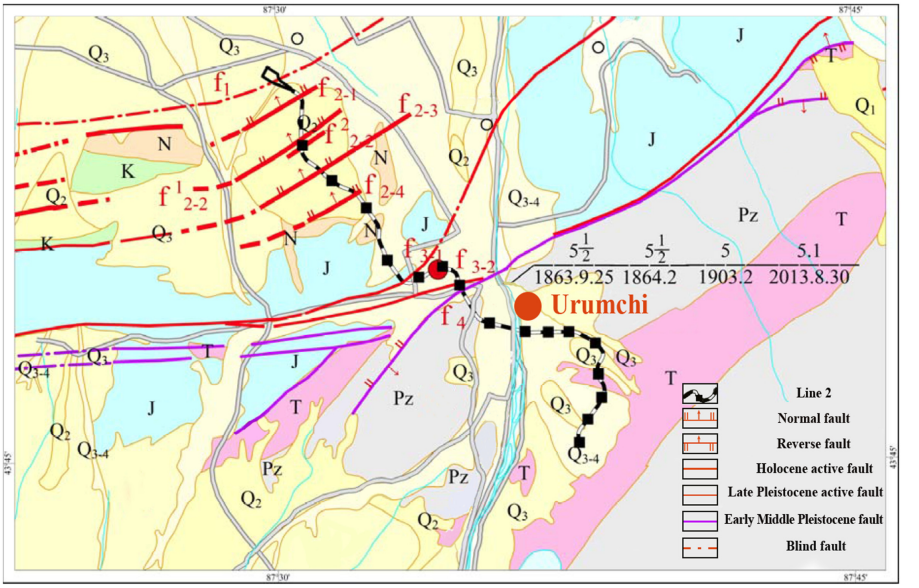

Figure 1.
Mapping of Line 2 and the fault plane in Urumqi rail transit

Note(s): F1: Bagang-Shihua buried fault; F2: Jiujiawan fault group; F3: Xishan fault; F4: Yamalik fault

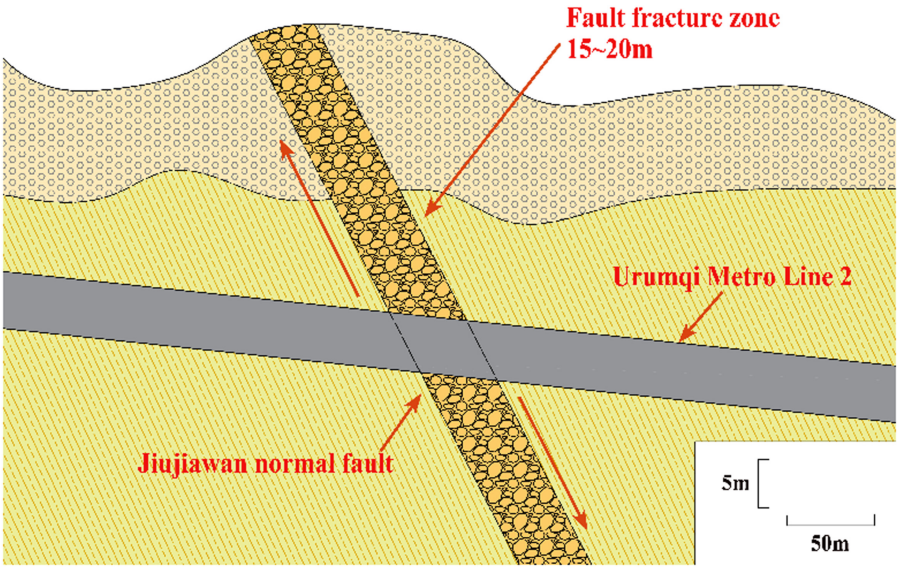

Figure 2.
Schematic of normal fault F_{j3} dislocation in Jiujiawan

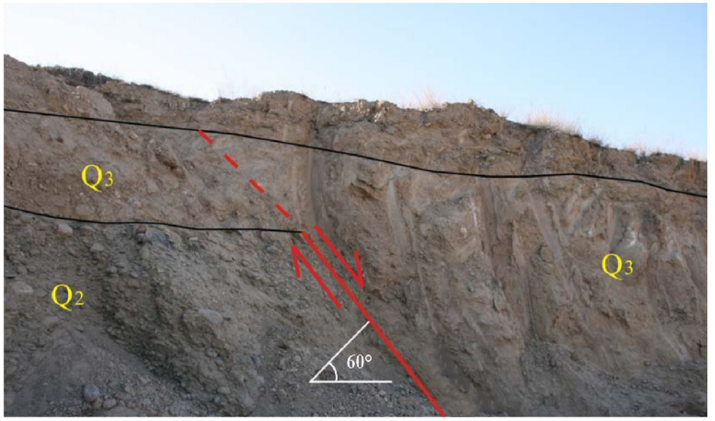

Figure 3.
Jiujiawan fault profile at the foundation pit under construction

material preparation is extensive; and although the general variation of the tunnel structure destruction can be observed, quantitative research is not sufficiently accurate. Considering the influence of the fault boundary conditions and the effect of gravity is often difficult with a small-scale model test when studying fault dislocation (Zhou *et al.*, 2022). Although a large-scale fault model test requires extensive labor and financial resources, more accurate quantitative analysis results can be obtained. Therefore, to study the failure characteristics of a tunnel structure under the condition of active fault dislocation, a test system is developed separately to simulate loading and fault rupture (Figure 4).

The model test system was designed to simulate loading and fault rupture (as shown in Figure 5a), which was monitored with a data acquisition and loading control system (as shown in Figure 5b). The loading model test system was mainly composed of the box body,

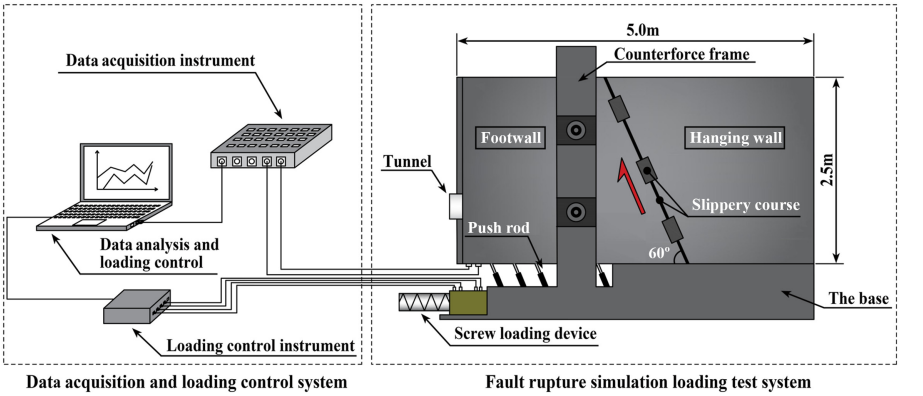

Figure 4.
Schematic diagram of the test system to simulate loading and fault rupture

a vertical screw loading device, a horizontal screw loading device, a thrust transmission device, a reaction frame and a base. The box body of the device (5 × 2.5 × 2.5 m) was provided with shear-slip joints of 60°, 75° and 90°. The bottom of the box was the base; and a reaction frame was fixed onto the base on both sides of the box. The high-power-high-speed screw loading system was installed underneath the bottom plate of the left footwall box body (as shown in Figure 5c), which caused the box body to move along the preset shear joints. The supporting computer digital servo control system controlled the screw loading rate and recorded the loading-time history curve. The system device had the following characteristics: (1) The large proportions and the size of the test device realized the coverage of the fault hanging wall, the footwall and tunnel structure within 125 m of the longitudinal range of the tunnel, ensuring the monitoring of the affected area of strata and tunnel structure under the simulation of fault dislocation, and provided better boundary conditions. (2) It realized multi-angle fault dislocation, and in the process of dislocation, the high-speed screw loading system provided a high-speed and stable loading rate, and the data acquisition system realized real-time monitoring of test data.

3.2 Similar material and model making

The test geometric similarity ratio was 1:25, the unit weight similarity ratio was 1:1 and the following physical quantities were calculated:

elastic modulus similarity ratio: 25,

Poisson's similarity ratio: 1,

stress similarity ratio: 25,

strain similarity ratio: 1,

earth pressure similarity ratio: 25 and

reinforcement amount: 625.

(1) Preparation of materials similar to the surrounding rocks

According to the physical and mechanical parameters of the actual surrounding rock, which were determined from the geological survey report of Jiujiawan's fault area and similar theories, the target values of similar material parameters were calculated, and the detailed parameters are shown in Table 1. According to the test results, the proportions (by weight) of

Test system to simulate loading and fault rupture

(a)

Data acquisition and loading control system

(b)

High-speed screw loading system

(c)

Figure 5.
Images of the test device and components for simulating loading and fault dislocation

similar materials in the surrounding rock were optimized as follows – river sand: quartz sand: coarse sand: fly ash: engine oil = 40%: 30%: 10%: 10%: 10%.

(2) The production of the plaster tunnel model

Certain proportions of water, gypsum and diatomaceous earth were mixed to prepare for the gypsum specimens (as shown in Figure 6), and two sets of annular and longitudinal strain gauges were passed onto the middle of the model. Then the loading test was carried out with the universal material testing machine. It tested each strength parameter and constantly adjusted the proportion for verification by adjusting the distribution ratio of each group. The final gypsum material ratio follows – water: gypsum: diatomaceous earth = 1.0: 0.7: 0.3; the detailed parameters are shown in Table 2.

The gypsum tunnel model was cast in an aluminum mold. The longitudinal lengths were 24 cm and 36 cm. The tunnel section types included the double-line box and double-line box arch. The cross-sectional size is shown in Figure 7. The gypsum tunnel model was reinforced by built-in steel mesh, which comprised 1 cm diameter steel bars spaced 10 cm apart.

Category	Density/(kN/m^3)	Elastic module/GPa	Poisson's ratio	Inner friction angle/°	Cohesion/MPa
Prototype	21	0.1	0.3	25	0.05
Model	21	0.0041	0.29	24.7	0.0021

Table 1.
Actual value and target value of surrounding rock material parameters

The gypsum tunnel model was demolded after pouring and maintained for 5–7 days to ensure its strength.

3.3 Experimental program

(1) Fault simulation program

Herein, with the Urumqi Metro Line 2 crossing the 60° normal fault of Jiujiawan as an example, the left side considered the footwall of the normal fault, and the right side was the hanging wall. The electric servo stimulated the screw loading device to lift the left footwall up along the 60°inclination-angle cutting deformation joint and enabled the soil in the box to achieve shear dislocation at the cutting deformation joint, thus simulating the dislocation effect of the normal fault on the tunnel structure. The tunnel burial depth was 52 cm, the soil thickness at the bottom of the tunnel was 60 cm and the entire tunnel model was composed of sections 1#–17#, as shown in Figure 8. Since the simulation of strike-slip dislocation has to rely on a higher dislocation rate, the loading rate was set at 5 mm/min, which was equivalent to the actual fault dislocation rate of 12.5 cm/min, and the loading target dislocation was 80 mm, equivalent to the 200 cm actual dislocation of the fault.

The actual width of the fault fracture zone is 15–20 m, and the ground survey work confirms that several repeated misalignments have occurred along the fault surface, so it is assumed that the fault misalignment still occurs along this surface in the test. Considering the mechanical properties of the fault surface, when the fault is repeatedly misshifted along the existing misshifted surface, the shear displacement will be limited to a narrow range near the misshifted surface, so the test is simplified to a sliding surface according to the survey results, using a double layer of PE (Polyethylene) plate simulation, between the plates coated with grease to help lubrication, PE plate reserved tunnel holes placed at the fault surface.

(2) Tunnel joint connection program

Prepared gypsum samples **(a)**

Loading samples **(b)**

Figure 6.
Testing the gypsum samples

Table 2.
Physical and mechanical parameters of the gypsum tunnel model

Category	Elastic module/GPa	Poisson's ratio	Axial compressive strength/MPa
Prototype	3.5	0.20	21.1
Model	1.30	0.194	0.802

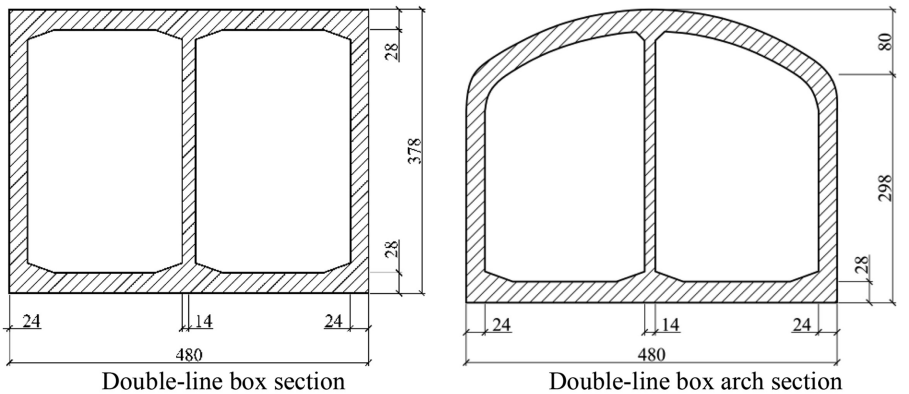

Figure 7.
Size of the cross sections (unit: mm)

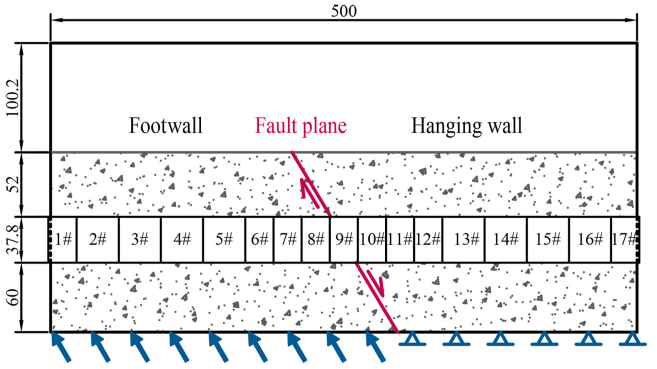

Figure 8.
Schematic diagram of the fault dislocation simulation (unit: cm)

In this model, two comparative test conditions using a double-line box section tunnel and an improved double-line box arch section tunnel were designed and conducted (as shown in Table 3). The longitudinal length of the plaster tunnel model was divided into 24 cm and 36 cm segments, and the T-section rubber ring was used to connect each segment (as shown in Figure 9). The rubber material was the same as the actual project EPDM (Ethylene Propylene Diene Monomer) rubber, and the material strength was customized by the manufacturer according to similar theoretical requirements. This special flexible, joint water-stop belt had strong elasticity, good water insulation, corrosion resistance and other advantages (see Table 4 for physical and mechanical parameters). It was applied to simulate the flexible hinged mode and water-stop belt connection between the sections and constituted a complete tunnel model with a total length of 5 m.

(3) Tunnel monitoring scheme

There were 19 monitoring sections along the length of the double-box tunnel and the double-box arch tunnel. The location and length of each section is shown in Figure 10. The test measurement contents included surface displacement, vertical displacement of the tunnel, longitudinal strain, circumferential strain and surrounding rock pressure.

Figure 11 shows the layout number and the location of the vertical displacement meter (including crown and baseplate), the longitudinal strain gauge (including crown and

Table 3.
Design of test conditions

Test case	Category	Segment lengths (cm)	Number of segments	Connector
1	Double-line box tunnel	24, 36	17	Special "T" shaped rubber ring
2	Double-line box arch tunnel	24, 36	17	Special "T" shaped rubber ring

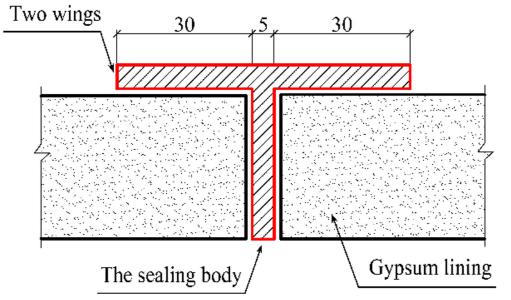

Special "T"-type rubber waterproof belt

(a)

Double-line box arch tunnel

(b)

Double-line box tunnel

(c)

Figure 9.
Segmented rubber waterproof belt connection of tunnel sections used in the model

	Unit	Index
Tensile strength	kPa	≥19.2
Tear strength	kN/m	≥1.2
Compression permanent deformation	%	≤15
Elongation at break	%	≥350

Table 4.
Physical and mechanical parameters of rubber material

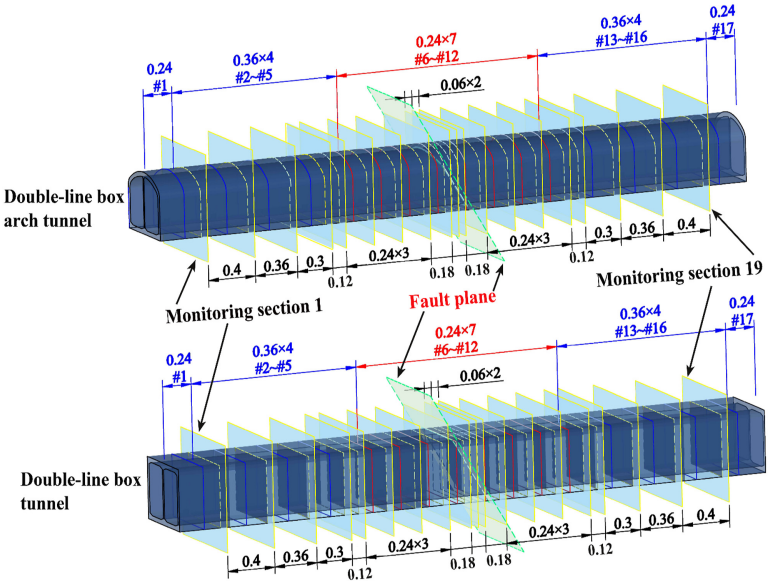

Figure 10.
Monitoring section layout and tunnel section length (unit: m)

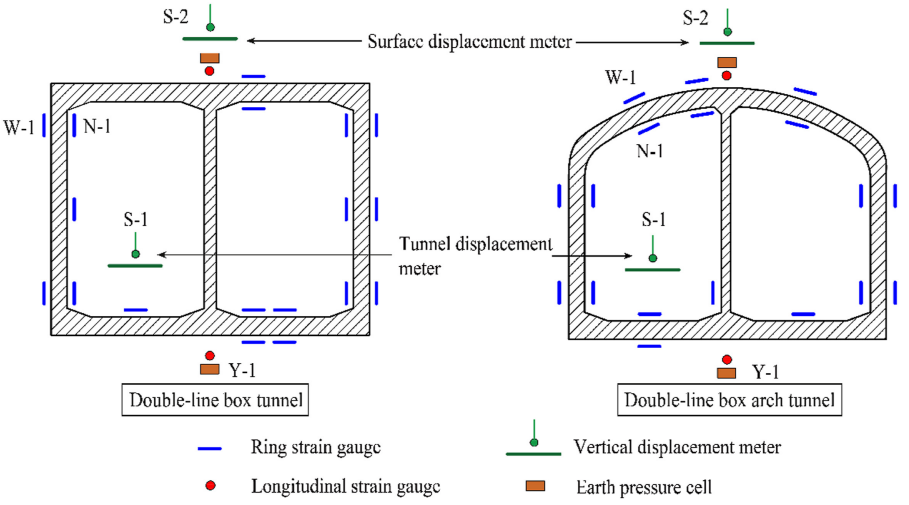

Figure 11.
Tunnel section component distribution

outside baseplate), the circumferential strain gauge (including section circumferential inner and outer) and the earth pressure box (including crown and outside baseplate) in each section.

4. Experimental results

The dynamic and static data acquisition system held a large amount of data. After data filtering and sorting, the curves of surface displacement, structural displacement,

longitudinal strain, hoop strain and surrounding rock pressure along the longitudinal position under 1.0–8.0 cm (equivalent to the actual 25–200 cm fault rupture and dislocation) offset were drawn. The experimental results were analyzed as follows.

4.1 Formation deformation law under fault dislocation

Figure 12 shows the vertical distribution curves of the ground displacement of the double-box tunnel and double-box arch tunnel. It can be seen from the diagram that during the fault dislocation, the footwall rose relatively, and the hanging wall was static. The vertical displacement of the surface was most obvious in the range −1.5–0.5 m, and the overall deformation was "S-shaped". With the increase in fault distance, the surface vertical displacement was also larger, but the maximum value was less than the fault momentum input value, indicating that a certain amount of strata compression occurred in the process of fault movement.

4.2 Forced deformation law of tunnel lining structure

Figure 13 shows the longitudinal distribution curves of the vertical displacement of the tunnel vault under the two cross-sectional types. It can be seen from the figure that the vertical displacement of the vault of the tunnel lining structure was mainly within the range −2.5–0.5 m (−5.2–1.1 D, D being the tunnel span), and the vertical displacement increased with the increase in the fault distance. The maximum vertical displacement of the double-line box tunnel vault was 6.8 cm (actual 170 cm dislocation momentum), and the maximum vertical displacement of the double-line box type arch tunnel vault was 7.1 cm

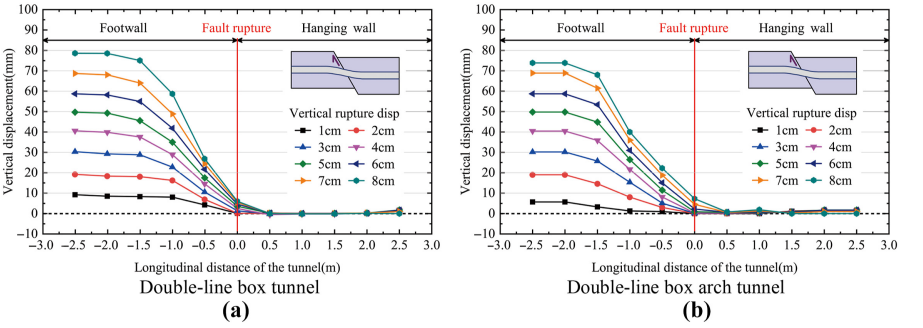

Figure 12.
Surface displacement curve

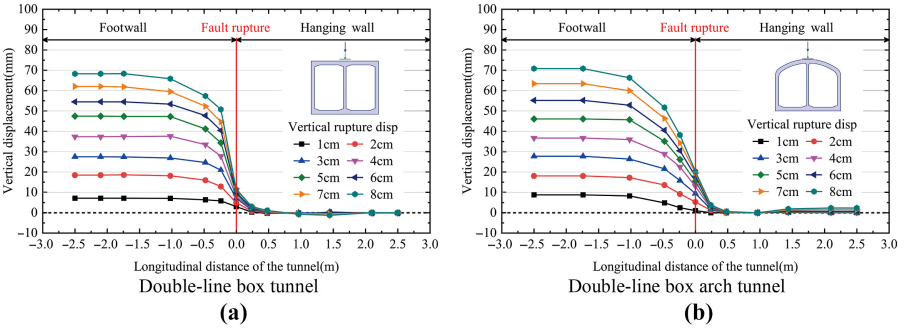

Figure 13.
Vertical displacement curve of vault

(actual 177.5 cm dislocation momentum). The maximum vertical displacement of the tunnel vault was less than the experimental dislocation amount of 8.0 cm (the actual dislocation amount of 2.00 m), owing to the compression between the stratum and the tunnel during the process of stratum uplift.

4.3 Longitudinal and lateral force characteristics and failure modes of tunnel lining structure

(1) Longitudinal strain

Figure 14a shows the variation curve of longitudinal strain along the longitudinal position outside the vault of the double-line box tunnel. It can be seen that the longitudinal strain of the vault fluctuated violently near the fault, and the range near the hanging wall fault plane increased significantly and was positive, indicating that this region was the main longitudinal tensile region of the vault, and the maximum longitudinal strain appeared at 0.05 m (0.1 D). When the fault distance reached 6.0 cm (actual fault distance of 150 cm), the longitudinal strain reached the maximum of 820 με, and when the fault distance exceeded 6 cm, the strain exceeded the range (2,000 με), indicating serious damage to the tunnel lining structure. In the range near the fault plane of the footwall, the longitudinal strain of the vault decreased significantly and was negative. The larger the fault distance, the smaller the strain value, indicating that the region was the longitudinal compression area of the vault. The minimum longitudinal strain occurred at −0.5 m (1.04 D), and when the fault distance reached 6.0 cm, the longitudinal strain reached the minimum value of −830 με. When the fault distance exceeded 6 cm, the strain increased significantly, indicating serious damage to the tunnel lining structure.

Figure 14b gives the distribution curve of the longitudinal strain outside the vault of the double-line box arch tunnel. The longitudinal strain of the vault fluctuated violently near the fault and increased rapidly in the range −0.24–0.24 m (−0.5–0.5 D) from the fault trace, indicating that the region was the main longitudinal tensile area of the vault, and the maximum longitudinal strain occurred at 0.06 m (0.125 D). When the fault distance reached 8.0 cm (actual 2.0 m fault distance), the longitudinal strain reached the maximum value of 52 με; in the range 0.24–1.0 m (0.5–2.1 D) from the hanging wall to the fault trace, the strain value was significantly reduced and negative. The larger the offset, the smaller the strain value, indicating that the region was the main longitudinal compression area of the vault; the minimum longitudinal strain appeared at 0.06 m (0.125 D), and the minimum was −42 με.

Compared with the double-line box tunnel, the peak strain of the double-line box arch tunnel was significantly reduced. The ultimate tensile strain of 106 με was used as the tensile failure standard. The analysis demonstrated that the longitudinal tensile strain of the double-

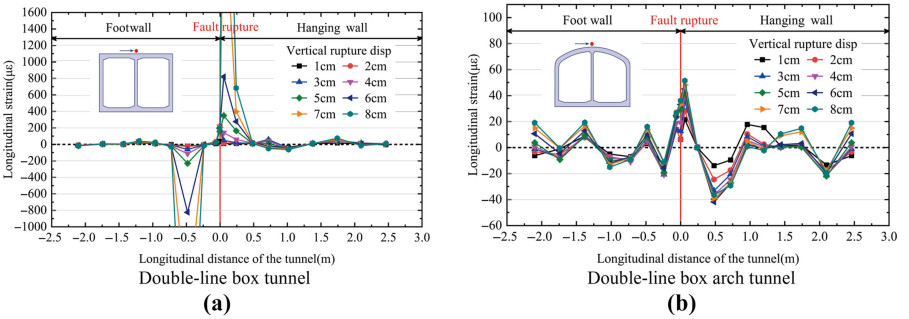

Figure 14.
Longitudinal strain curve outside vault

line box tunnel structure greatly exceeded the ultimate tensile strain and that longitudinal tensile failure would occur. Considering the longitudinal bending deformation characteristics of the tunnel structure, the failure mode of the longitudinal tensile strain overrun area was determined to be tensile-bending failure, and its failure mode is shown in Figure 15.

(2) Hoop strain

Figure 16a shows the variation curve of the circumferential strain along the longitudinal position on the inner side of the baseplate of the double-line box tunnel. It can be seen that the circumferential strain on the inner side of the floor of the left tunnel increased significantly near the fault plane of the hanging wall. When the fault distance exceeded 2.0 cm (the actual fault distance of 50 cm), the circumferential strain on the inner side of the baseplate at the fault trace reached 340 με, which exceeded the ultimate tensile strain of 106 με. The lining was subjected to tensile failure, which was manifested as the longitudinal crack on the inner side of the baseplate. Then, with the increase in the offset, the circumferential strain on the inner side of the floor continued to increase. When the fault distance reached 8 cm (the actual fault distance of 200 cm), the circumferential strain on the inner side of the baseplate reached the maximum of 860 με.

Figure 16b shows the distribution curve of the circumferential strain inside the baseplate of the double-line box arch tunnel. The circumferential strain inside the baseplate significantly decreased and was negative in the range −0.48–0.0 m (−1.0–0 D) from the fault trace in the footwall, indicating that the baseplate inside the region was in a longitudinal compression state. In the hanging wall from the fault trace, the baseplate range increased significantly, 0.48–0.0 m (1.0–0 D), and was a positive value, indicating that the inner baseplate in the region was in a longitudinal tensile state. When the offset exceeded 2.0 cm (actual 50 cm offset), the peak circumferential strain of the inner side of the baseplate in the

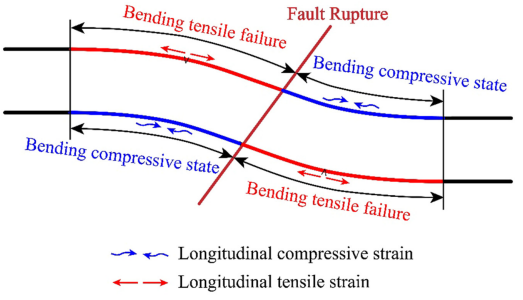

Figure 15.
Diagram of the longitudinal tensile-bending failure mode of tunnel lining

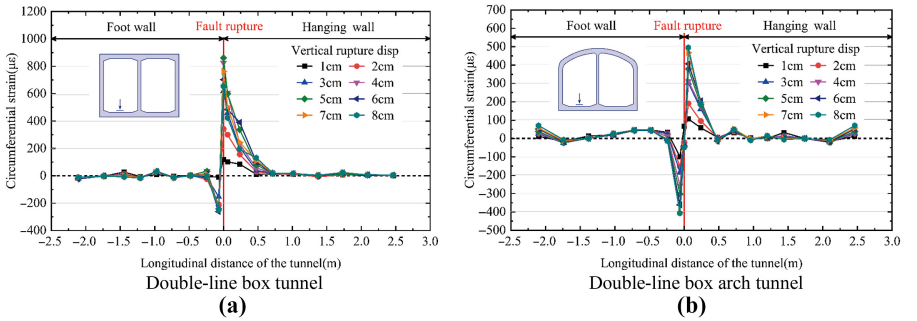

Figure 16.
Circumferential strain curve inside the baseplate

hanging wall near the fault reached 190.9 με, which exceeded the ultimate tensile strain of the structure by 106 με. It was concluded that the lining was subjected to tensile damage, which was manifested as longitudinal cracks in the inner side of the baseplate. Then, the circumferential strain continued to increase with the increase in the offset. When the offset reached 8.0 cm (actual 150 cm offset), the maximum circumferential strain of the inner side of the inverted arch reached 495.3 με.

Compared with the double-line box tunnel, the peak circumferential strain of the double-line box arch tunnel was significantly reduced, and the maximum tensile strain was reduced by 42.4%. Using the ultimate tensile strain of 106 με as the standard analysis for the tensile damage, it can be seen that when the offset exceeds 2.0 cm (the actual offset is 50 cm), the circumferential strain of the double-line box tunnel exceeds 340 με, and the strain increases sharply with the increase of the offset. In contrast, the strain of the double-line box arch tunnel exceeds 190.9 με, and the strain increases less with the increase of offset. It indicates that the circumferential tensile strains at the fracture surface of both section types of tunnel structures exceed the allowable values, and large eccentric tensile damage occurs at the section, and longitudinal cracks will appear. The damage mode is shown in Figure 17.

4.4 Surrounding rock pressure

Figure 18 shows the variation curves of the surrounding rock pressure along the longitudinal position of the crown and the baseplate of the box tunnel. As seen in the figure, the surrounding rock pressure of the crown increased rapidly in the range −0.5–−0.25 m (−1.04–−0.52 D), and the maximum value appeared at −0.24 m from the fault trace in the footwall. With the increase in the offset, the peak value of the surrounding rock pressure was also larger. When the offset reached 4.0 cm (the actual 100 cm offset momentum), the maximum value reached 20 kPa. With the further increase in the offset, the soil on the tunnel in the fault zone was loosened and voided from the influence of the fault movement, resulting in the rapid

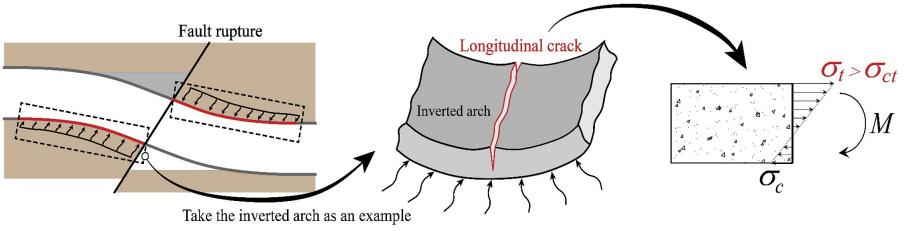

Figure 17.
Schematic diagram of large eccentric tension damage on the cross-section of the tunnel structure

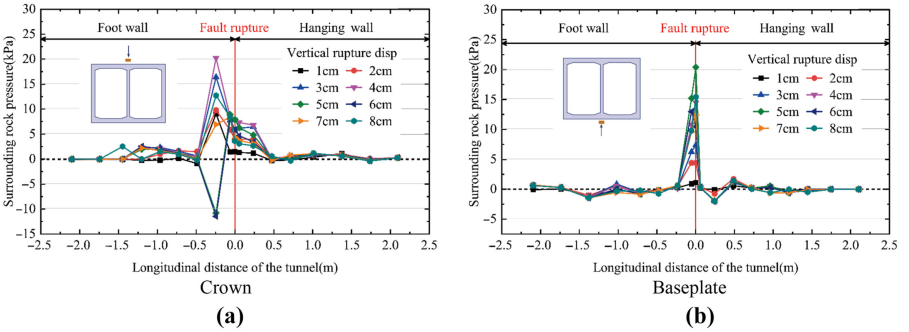

Figure 18.
Pressure curve of rock surrounding the double-line box tunnel

decrease in soil pressure. When the offset reached 6 cm (the actual offset was 150 cm), the soil pressure dropped to the minimum value of −11.5 kPa.

The baseplate soil pressure increased rapidly and was positive near the fault trace in the footwall, reaching the maximum value of 20.4 kPa when the offset reached 4 cm (actual 100 cm offset). The soil pressure decreased rapidly and remained constant within a certain range after the tunnel has crossed the fault zone.

Figure 19 illustrates the longitudinal distribution curve of the surrounding rock pressure of the crown and baseplate of the double-line box arch tunnel. In the figure, it can be seen that the surrounding rock pressure of the crown decreased and was negative in the range −0.76–−0.24 m (−1.5–−0.5 D) from the fault trace and reached the minimum value at −0.48 m (1.0 D) from the fault trace in the footwall. The minimum value was −17.3 kPa, indicating that the crown of the region was partially empty. It increased rapidly in the range −0.24–0.48 m (−0.5–1.0 D) from the fault trace, and the peak value of surrounding rock pressure appeared at the fault plane. The larger the offset, the greater the peak value and the maximum value reached 41.2 kPa (1.03 MPa) when the offset reached 5.0 cm (actual 200 cm offset).

The surrounding rock pressure of the baseplate increased rapidly and was positive in the range −1.02–0 m (−2.13–0 D) from the fault trace, reaching the maximum value of 57.7 kPa (1.44 MPa) at −0.06 m (−0.125 D) from the fault plane. The pressure of the surrounding rock decreased rapidly in the range 0–0.48 m (0–1.0 D) from the fault trace in the hanging wall, and the surrounding rock pressure was stabilized at the minimum value of −26.7 kPa in the range 0.06–0.24 m (0.125–0.5 D), indicating that the inverted arch lining and surrounding rock were completely separated in this range.

The analysis demonstrated that the lengths of the void areas of the hanging wall and footwall were all about 0.4 m in the dislocation process of the double-line box tunnel. In the dislocation process of the double-line box arch tunnel, the length of the void area of the hanging wall was approximately 0.4 m, and that of the footwall 0.5 m, indicating that the tunnel section type had little effect on the range of the void area.

4.5 Crack characteristics analysis of tunnel lining structure

4.5.1 Double-line box tunnel. Figure 20 shows the damage pattern of the double-line box tunnel lining at the end of the test. According to the distribution of tunnel cracks, the continuous crack expansion diagram of each segment is drawn, as shown in Figure 21. The crack pattern, number of cracks and crack locations are summarized in Table 5.

(1) Cracks appeared in the #7–#12 segments of the tunnel lining, with only longitudinal cracks.

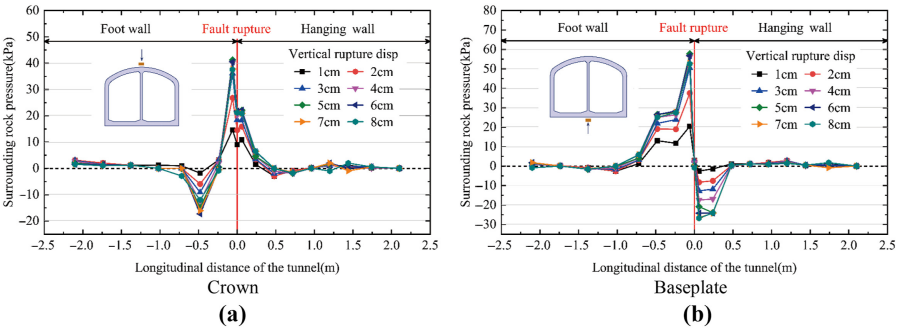

Figure 19.
Pressure curve of rock surrounding the double-line box arch tunnel

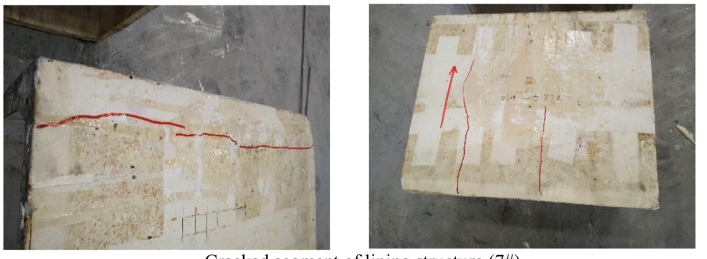

Cracked segment of lining structure (7#)

(a)

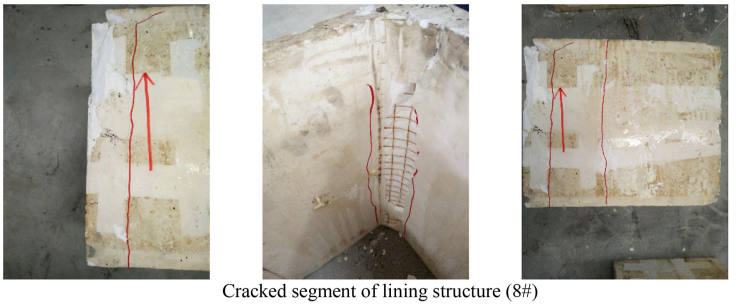

Cracked segment of lining structure (8#)

(b)

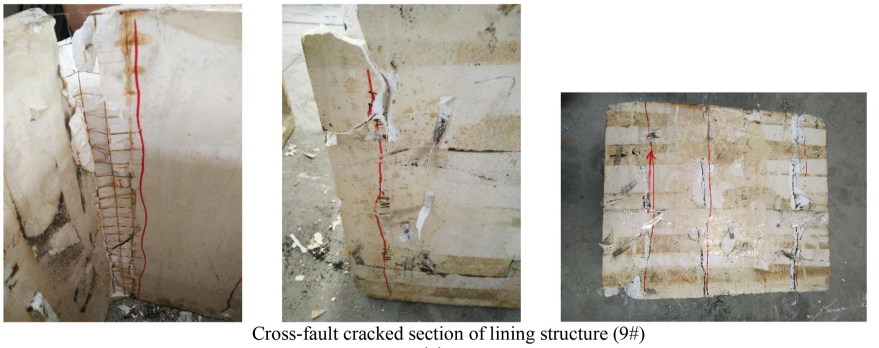

Cross-fault cracked section of lining structure (9#)

(c)

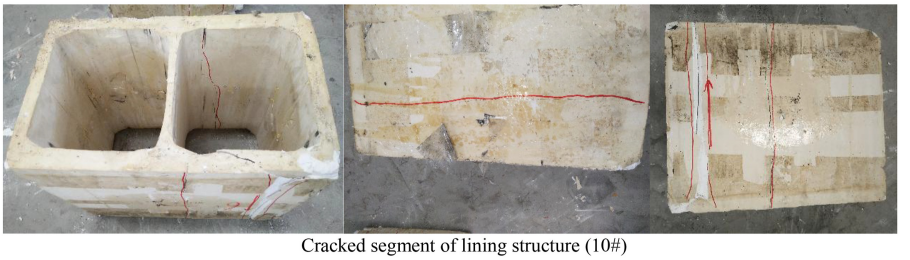

Cracked segment of lining structure (10#)

(d)

Figure 20.
Tunnel segment cracking

Cracked segment of lining structure (11#)

(e)

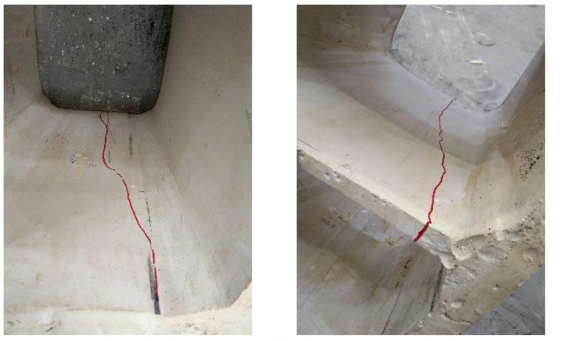

Cracked segment of lining structure (12#)

(f)

Figure 20.

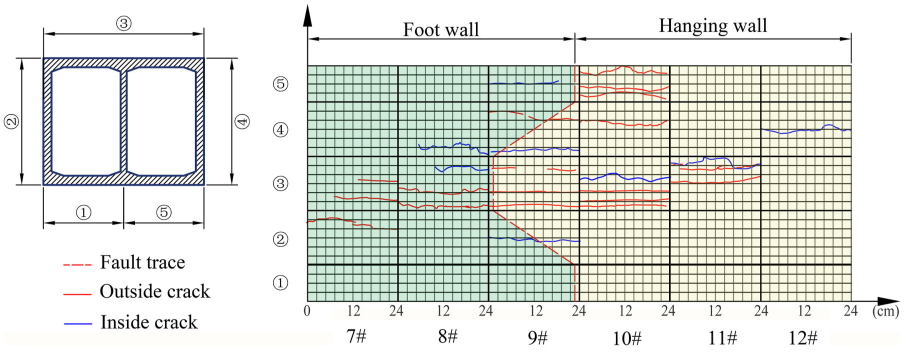

Figure 21.
Tunnel crack expansion diagram

(2) The largest number of cracks and the most serious damage were found in the #9 segments, which were affected by the direct shear of the fault surface.

(3) The longitudinal crack depth was the largest in the #9–#10 segments, and there were many fractures along the longitudinal cracks. The longitudinal fractures were mainly concentrated at the intersection angle of the middle wall with the baseplate and roof, accompanied by a large number of spalling blocks and obvious exposure of the reinforcement mesh. There were also obvious longitudinal cracks at the middle wall. Since the middle wall and multiple right-angle structures improved the shear and

Tunnel segment number	Quantity	Crack distribution characteristics Longitudinal cracks Position	Total length of cracks/cm
#7	3	Roof, upper left corner	62
#8	4	Roof, upper right corner	109
#9	9	Roof, baseplate, upper right corner	228
#10	8	Baseplate, lower left corner, lower right corner	206
#11	4	Baseplate, lower left corner, lower right corner	105
#12	2	Lower left corner	56
Summary	30	Roof, baseplate lower left corner, four corners	766
Damage type	Mainly large eccentricity damage		
Cracking range	The hanging wall cracking range is 140 cm (2.92 D), the footwall cracking range is 96 cm (2.0 D). The damage scope of the hanging wall is obviously larger than that of the footwall		

Table 5.
Double-line box tunnel lining crack pattern and quantity statistics

longitudinal bending resistance of the tunnel lining structure, no oblique cracks (shear cracks) and circumferential cracks developed during the test.

(4) The damage range of the tunnel structure in the hanging wall was significantly larger than that of the footwall. When the staggered distance reached 8.0 cm (actual 200 cm misalignment), the damage range of the tunnel structure in the hanging wall was about 140 cm, and the damage range of the tunnel structure in the footwall was about 100 cm.

4.5.2 Double-line box arch tunnel. Figure 22 shows the damage pattern of the structure of the double-line box arch tunnel at the end of the test. According to the distribution of tunnel cracks, the continuous crack expansion diagram of each segment is drawn, as shown in Figure 23. The crack pattern, number of cracks and crack locations are summarized in Table 6.

(1) Cracks appeared in the #7–#12 segments of the tunnel lining, with longitudinal cracks dominating. The cracks mainly appeared on the inside and outside of the baseplate, the outside of the wall foot and the outside of the arch foot.

(2) The location of longitudinal cracks was basically consistent with the longitudinal distribution of surrounding rock pressure, indicating that the large local load on the cross-section caused an excessive local bending moment in the structure. The tunnel lining structure suffered large eccentric damage and formed longitudinal cracks.

(3) The middle wall improved the shear and longitudinal bending resistance of the lining structure. There were no oblique cracks (shear cracks) and circumferential cracks after the test. However, owing to the existence of the straight wall foot structure, the stress concentration at the wall foot was obvious, so the number of longitudinal cracks at the wall foot and baseplate was the largest.

(4) The damage range of the tunnel structure in the hanging wall was significantly larger than that of the footwall. When the staggered distance reached 8.0 cm (actual 200 cm misalignment), the damage range of the tunnel structure in the hanging wall was about 84 cm, and the damage range of the tunnel structure in the footwall was about 60 cm.

It can be seen from Figures 21 and 23 that the damage degree of the double-line box tunnel is obviously serious compared with the double-line box arch tunnel. The length and number of

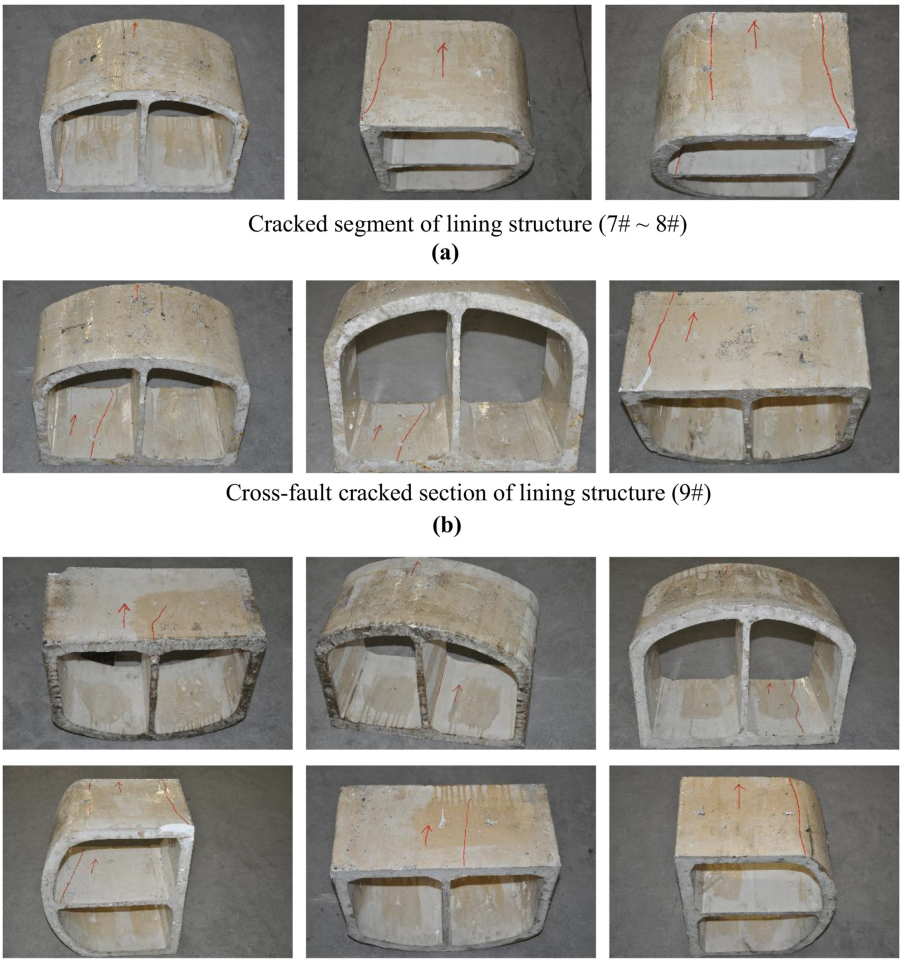

Figure 22.
Tunnel segment cracking

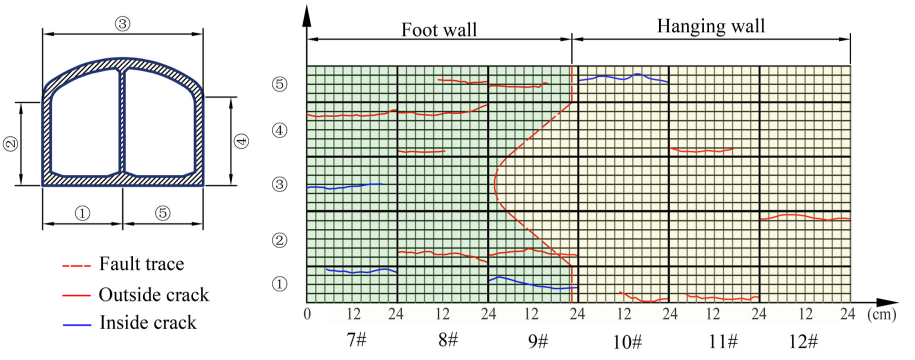

Figure 23.
Tunnel crack expansion diagram

Tunnel segment number	Crack distribution characteristics Quantity	Longitudinal cracks Position	Total length of cracks/cm
7#	3	Left wall foot, right wall foot	60
8#	5	Right arch foot, right wall foot, top of middle column, baseplate	85
9#	3	Baseplate, left arch foot	56
10#	2	Inside and outside of baseplate	48
11#	2	Baseplate, bottom of middle column	36
12#	1	Inside of baseplate	26
Summary	14	Damage mainly concentrated in: inside and outside bottom plant, outside wall foot, outside arch foot	311
Damage type	Mainly large eccentricity damage		
Cracking range	The hanging wall cracking range is 3.5 segments, 84 cm (1.75 D), and the footwall cracking range is 2.5 segments, 60 cm (1.25 D). The damage scope of the hanging wall is obviously larger than that of the footwall; the crack length of the hanging wall is 225 cm and that of the footwall is 86 cm. The damage degree of the hanging wall is greater than that of the footwall		

Table 6.
Double-line box arch tunnel lining crack pattern and quantity statistics

cracks in the lining failure are much larger than those in the double-line box arch tunnel. The failure segments of the double-line box arch tunnel are mainly concentrated in 8#, 9# and 10#, while the failure segments of the double-line box arch tunnel are mainly concentrated in 7#, 8# and 9#. In terms of fracture morphology, the longitudinal fracture is the main failure mode of the two sections of tunnels, which indicates that the failure mode is the large eccentric tensile failure. In practical engineering, it should be considered to add the circumferential reinforcement.

Analyzing the effect of the anti-staggering of the two section forms, the damage range and damage degrees for the double-line box tunnel and the double-line box arch tunnel are summarized as shown in Table 7. Compared with the box tunnel, the damage ranges for both the hanging wall and footwall of the improved box arch tunnel were significantly reduced, where the damage range of the hanging wall was reduced by 40%, and the damage range of the footwall was reduced by 37.5%, for a total damage range reduction of about 39%. The damage degree in the box arch tunnel was also significantly reduced. As seen in the crack diagram, the total crack length was reduced by 59.3%, and there was no obvious spalling or block falling. This indicated that the improved two-line box arch tunnel had better resistance to misalignment.

The analysis of the above test results shows that the improved double-line box arch tunnel has better resistance to misalignment, but there are still more longitudinal cracks in the lining crack map after the test. Therefore, in the actual project, the number of hoop bars should be considered to be increased in the tunnel-fault intersection area to reduce the longitudinal

Type	Damage range Hanging wall (cm)	Footwall (cm)	Total (cm)	Damage degree Crack length (cm)	With or without spalling and block falling
Double-line box tunnel	14	96	236	766	Apparent spalling and block falling
Double-line box arch tunnel	84	60	144	311	No spalling

Table 7.
Comparative analysis of antistaggering effect

cracks generated by large eccentric tensile damage. Analysis of the change in the pressure of the surrounding rock shows that a certain number of soil de-hollowing areas will appear at the vicinity of the fault; therefore, after the fault displacement occurs, the cavity area should be backfilled or reinforced to facilitate rapid repair work and subsequent restoration and reinforcement.

5. Conclusion

In this paper, the open excavation section of Urumqi Metro Line 2 crossing the Jiujiawan 60° normal fault was taken as the engineering background. Based on a large-scale physical model test, we compared and analyzed the mechanical behavior differences between two types of tunnel lining sections: open-cut double-line box and modified double-line box arch. Moreover, we studied in depth the mechanical characteristics and damage morphology of the tunnel structures of the two section types; the main conclusions are as follows:

(1) Under the effect of fault misalignment, both cut-and-cover double-line box tunnels and modified double-line box arch tunnels were dominated by large eccentric damage owing to the improved overall flexibility of segmental tunnels and the shear and bending resistance of the diaphragm walls in the box sections. The test process showed that only longitudinal cracks appeared in the tunnel lining structure and that no circumferential cracks appeared, which indicated a good ability to adapt to deformation.

(2) Compared with the ordinary box tunnel, the damage extent and damage degree of the hanging wall and the footwall of the improved box arch tunnel were significantly reduced. Between them, the extent of the damage was reduced by about 39%, the total crack length was reduced by about 59.3% and there was no obvious spalling or falling blocks. This indicated that the improved double-line box arch tunnel had better resistance to misalignment.

(3) Under the condition that the cut-and-cover tunnel crosses the active normal fault, the damage range of the hanging wall of the box section tunnel was 140 cm, and the damage range of the footwall was 96 cm. The damage range of the hanging wall of the box arch tunnel was 84 cm and the damage range of the footwall was 40 cm. In addition, the number of cracks in the hanging wall was significantly larger than those in the footwall. Therefore, the extent of damage to the hanging wall tunnel structure and the damage degree were significantly greater than that to the footwall tunnel structure.

(4) As the tunnel lining structure of the cut-and-cover section and the double-line box arch tunnel structure improved the shear and longitudinal bending resistance of the structure. The top arch structure was better in the stress performance than the straight arch structure. However, the stress concentration at the foot of the straight wall made the wall foot and the floor face greater safety risks. Therefore, consideration should be given to increasing the number of circumferential main reinforcements in the lining structure at the wall foot and the floor to reduce the generation of longitudinal cracks.

References

Abers, G. A. (2009). Slip on shallow-dipping normal faults. *Geology*, *37*, 767–768. doi: 10.1130/focus082009.1.

Allen, C. R., Luo, Z. L., Qian, H., Wen, X. Z., Zhou, H. W., & Huang, W. S. (1991). Field study of a highly active fault zone: The Xianshuihe fault of Southwestern China. *Geological Society of America Bulletin*, *103*, 1178–1199. doi: 10.1130/0016-7606(1991)1032.3.CO;2.

Anastasopoulos, I., Gazetas, G., Bransby, M., Davies, M., & El Nahas, A. (2007). Fault rupture propagation through sand: Finite-element analysis and validation through centrifuge experiments. *Journal of Geotechnical and Geoenvironmental Engineering*, *133*, 943–958. doi: 10.1061/(ASCE)1090-0241(2007)133:8(943).

Anastasopoulos, I., Gerolymos, N., Drosos, V., Georgarakos, T., Kourkoulis, R., & Gazetas, G. (2008). Behaviour of deep immersed tunnel under combined normal fault rupture deformation and subsequent seismic shaking. *Bulletin of Earthquake Enginerring*, *6*, 213–239. doi: 10.1007/s10518-007-9055-0.

Bray, J. D., Seed, R. B., Ciuff, L. S., & Seed, H. B. (1994). Earthquake fault rupture propagation through soil. *Journal of Geotechnical Engineering-ASCE*. doi: 10.1016/0148-9062(94)90065-5.

Burridge, P. B., Scott, R. F., & Hall, J. F. (1989). Centrifuge study of faulting effects on tunnel. *Journal of Geotechnical Engineering*, *115*, 949–967. doi: 10.1016/0148-9062(90)90407-s.

Byerlee, J. D., & Brace, W. F. (1968). Stick slip, stable sliding, and earthquakes—effect of rock type, pressure, strain rate, and stiffness. *Journal of Geophysical Research*, *73*, 6031–6037. doi: 10.1029/jb073i018p06031.

Cui, G. (2014). The seismic design calculation method and test study of tunnel shallow-buried portal and rupture stick-slipping section. *Chinese Journal of Rock Mechanics and Engineering*, *33*, 648. doi: 10.13722/j.cnki.jrme.2014.03.026.

Johansson, J., & Konagai, K. (2007). Fault induced permanent ground deformations: Experimental verification of wet and dry soil, numerical findings' relation to field observations of tunnel damage and implications for design. *Soil Dynamics and Earthquake Engineering*, *27*(10), 938–956. doi: 10.1016/j.soildyn.2007.01.007.

Jeon, S., Kim, J., Seo, Y., & Hong, C. (2004). Effect of A fault and weak plane on the stability of A tunnel in rock—a scaled model test and numerical analysis. *Journal of Rock Mechanics and Mining Sciences*, *41*(Supplement l), 321–326. doi: 10.1016/j.ijrmms.2004.03.115.

Jiang, S., Li, P., & Lin, Z. (2008). Design strategies of breaking resistance of tunnels crossing arctive faults zone. *Journal of Chongqing Jiaotong University (Natural Science)*, *6*, 1034–1036, 1041 (in Chinese).

Karamitros, D. K., Bouckovalas, G. D., & Kouretzis, G. P. (2007). Stress analysis of buried steel pipelines at strike-slip fault crossings. *Soil Dynamics and Earthquake Engineering*, *27*, 200–211. doi: 10.1016/j.soildyn.2006.08.001.

Kim, N. Y., Park, D. H., Jung, H. S., & Kim, M. I. (2020). Deformation characteristics of tunnel bottom after construction under geological conditions of long-term deformation. *Geomechanics and Engineering*, *21*(2), 171–178. doi: 10.12989/gae.2020.21.2.171.

Lecomte, E., Le Pourhiet, L., & Lacombe, O. (2012). Mechanical basis for slip along low-angle normal faults. *Geophysical Research Letters*, *39*(3), L03307. doi: 10.1029/2011gl050756.

Lee, J. W., & Hamada, M. (2005). An experimental study on earthquake fault rupture propagation through a sandy soil deposit. *Structural Engineering/Earthquake Engineering*, *22*, 1–13. doi: 10.2208/jscej.2005.780_1.

Lin, M. -L., Chung, C. -F., & Jeng, F. -S. (2006). Deformation of overburden soil induced by thrust fault slip. *Engineering Geology*, *88*, 70–89. doi: 10.1016/j.enggeo.2006.08.004.

Liu, X. Z., Li, X. F., Sang, Y. L., & Lin, L. L. (2015). Experimental study on normal fault rupture propagation in loose strata and its impact on mountain tunnels. *Tunnelling and Underground Space Technology*, *49*, 417–425. doi: 10.1016/j.tust.2015.05.010.

Mcgarr, A., & Fletcher, J. B. (2003). Maximum slip in earthquake fault zones, apparent stress, and stick-slip friction. *Bulletin of the Seismological Society of America*, *93*, 2355–2362. doi: 10.1785/0120030037.

Ohnaka, M. (1973). Experimental studies of stick-slip and their application to the earthquake source mechanism. *Journal of Physics of the Earth*, *21*, 285–303. doi: 10.4294/jpe1952.21.285.

Roth, W. H., Scott, R. F., & Austin, I. (1981). Centrifuge modeling of fault propagation through alluvial soils. *Geophysical Research Letters*, *8*, 561–564. doi: 10.1029/gl008i006p00561.

Shahidi, A. R., & Vafaeian, M. (2005). Analysis of longitudinal profile of the tunnels in the active faulted zone and designing the flexible lining (for Koohrang-III tunnel). *Tunnelling and Underground Space Technology*, *20*, 213–221. doi: 10.1016/j.tust.2004.08.003.

Sibson, R. H. (1977). Fault rocks and fault mechanisms. *Journal of the Geological Society*, *133*, 191–213. doi: 10.1144/gsjgs.133.3.0191.

Süleyman, D. (2002). Tunneling in squeezing rock, the Bolu tunnel. *Anatolian Motorway, Turkey, Engineering Geology*, *67*, 73–96. doi: 10.1016/S0013-7952(02)00146-1.

Taniyama, H., & Watanabe, H. (2002). Deformation of sandy deposits by reverse faulting. *Structural Engineering/Earthquake Engineering*, *19*, 209–219. doi: 10.2208/jsceseee.19.209s.

Wang, Y. Q., Chang, H. T., Wang, J. Y., & Qiu, J. L. (2019). Countermeasures to treat collapse during the construction of road tunnel in fault zone: A case study from the Yezhuping tunnel in south Qinling, China. *Environmental Earth Sciences*, *78*(15). doi: 10.1007/s12665-019-8481-z.

Zhang, N., Shen, J. S., Zhou, A., & Arulrajah, A. (2018). Tunneling induced geohazards in mylonitic rock faults with rich groundwater: A case study in Guangzhou. *Tunneling & Underground Space Technology*, *74*, 262–272. doi: 10.1016/j.tust.2017.12.021.

Zhao, X., & Yang, X. H. (2019). Experimental study on water inflow characteristics of tunnel in the fault fracture zone. *Arabian Journal of Geosciences*, *12*(13). doi: 10.1007/s12517-019-4561-3.

Zheng, S., Jiang, S., & Li, P. (2013). The damage characteristics and protection methods of tunnel cross active fault zone. *Highway Engineering*, *4*(25-28), 33 (in Chinese).

Zhou, G. X., Sheng, Q., Cui, Z., Wang, T. Q., Ma, Y. L. N., & Fu, X. W. (2022). Model test of failure mechanism of tunnel with flexible joint crossing active fault under strike-slip fault dislocation. *Rock and Soil Mechanics*, *43*(1), 37–50. doi: 10.16285/j.rsm.2021.0765.

Corresponding author
Zhiqiang Zhang can be contacted at: 214317032@qq.com